Gas flow assisted powder deposition for enhanced flowability of fine powders: 3D printing of α-tricalcium phosphate

Fabio Chinellato [a,b], Janka Wilbig [a,*], Dominik Al-Sabbagh [a], Paolo Colombo [b], Jens Günster [a]

[a] *Bundesanstalt für Materialforschung und -prüfung, Unter Den Eichen 44-46, 12203, Berlin, Germany*
[b] *Dipartimento di Ingegneria Industriale, University of Padova, Via Marzolo 9, 35131, Padova, Italy*

ARTICLE INFO

ABSTRACT

The possibility of creating patient-specific individual implants makes Additive Manufacturing technologies of special interest for the medical sector. For substitution of bone defects, powder based Additive Manufacturing by Binder Jetting is a suitable method to produce complex scaffold-like structures made of bioceramics with easily adapted geometries and controlled porosity. The process inherent residual porosity in the printed part, even though desired as it supports bone ingrowth, also leads to limited mechanical strength. Currently, bioceramic scaffolds made by Binder Jetting feature suitable biocompatible and biodegradable properties, while a sufficient mechanical stability is rather challenging. The purpose of this work is to apply the *gas flow assisted powder deposition* introduced in 2014 by Zocca et al., to the powder bed during printing of bioceramic tablets and scaffolds using α-TCP powder as feedstock. This enables exploiting the advantages of an increased powder bed density, thereby improving the mechanical properties of the printed parts.

1. Introduction

Additive Manufacturing technologies, which allow to produce complex geometries layer by layer, have found their way into various areas of the medical sector for quite some time. Metal implants, like spine cages or polymeric hearing aids, are only two of many examples of the successful use of Additive Manufacturing (AM) for medical applications. Many more are currently the object of extensive research such as scaffold structures for tissue engineering applications or bone substitution and restoration. [1] Scaffolds are, in general, three dimensional support structures which allow the infiltration of cells, thereby supporting cell proliferation and differentiation. These phenomena are strictly connected to the material of the scaffolds (that has to be biocompatible and customized depending on the application) and its porosity (that is essential to ensure sufficient oxygen, nutrients and also waste diffusion throughout the implant). Unlike other conventional techniques, AM technologies have significant advantages in this field. Indeed, the geometrical porosity can be efficiently controlled by the CAD design while the porosity of the solid depends on the particle size distribution of the feedstock chosen as well as on printing process parameter. [2] Particularly interesting for this application is the *Binder Jetting (BJ)* process as defined in the ISO standard DIN EN ISO 17296–2:2016.

Particles of the powder bed are connected via a typically organic binding liquid that is applied layer by layer by nozzles of a print head according to the specific geometry desired. The resulting green part is cleaned from residual loose powder and heat treated afterwards for burnout of the binder and sintering. To produce scaffolds that mimic and co-operate with the natural bone, bioceramics are often used due to its mineral structure similar to natural bone. Calcium phosphates constitute the important biomineral phase in the human body, and the bone mineral contains about 85% of Hydroxyapatite (HA). Therefore, calcium phosphates are ideal for bone repair and in particular tricalcium phosphate that not only is biocompatible and bioactive but also bioresorbable. Its degradation allows the natural bone to recover. Critical size defects, which require bone substitution to avoid nonunions and malunions can be caused by traumas like fractures or diseases like bone cancer for instance. [3,4,5] Tricalcium phosphate has three polymorphs, of which two are relevant and widely used in the medical sector: β-TCP, which is stable below 1125°C and α-TCP, which occurs when heating β-TCP above 1125°C. The third phase α'-TCP lacks of practical interest as it occurs above 1400°C and reverts into α-TCP during cooling. The theoretical density of these phases changes from 3.066 g/cm^3 for β-TCP to 2.866 g/cm^3 for α-TCP and 2.702 g/cm^3 (α'-TCP). [6] Both α- and β-TCP are currently employed in many clinical practices in dentistry, maxillo-facial

---

surgery and orthopedics for bone repair and remodeling, typically in the shape of granules or powder [6]. In literature, α-TCP is considered to be more degradable than β-TCP [6,7]. The reason is related to the lower density of α-TCP compared to β-TCP since a weaker lattice structure promotes a faster degradation. Therefore, α-TCP in particular can be of interest to tailor degradation rates as well as biodegradable carriers for the controlled release of drugs [6]. The good biological properties of these materials are well established, but significant limitations for the use of scaffolds made of calcium phosphates result from their limited mechanical properties, due to high brittleness and low fatigue strength. An approach for achieving improved mechanical properties through the control of the residual porosity is the manufacturing of scaffolds using BJ in combination with *gas flow assisted powder deposition*. 3D printing of tricalcium phosphate has already been described in the literature, focusing mainly on β-TCP (cf [8]). To further understand the processability and sintering behaviour of 3D printed scaffolds made of α-TCP, this material was chosen for the process evaluation. To process a material via Binder Jetting, it should be available in powder form, and it must be flowable. The typical particle size of a powder which is suitable to process without gas flow is between 45 - 100 μm. With smaller particle sizes, especially smaller than 25 μm the successful deposition of defect-free powder layers becomes challenging. In fact, a homogenous powder distribution in the powder bed is normally not possible, as fine powder tends to agglomerate due to the dominating interparticle forces. However, using smaller particles would come with advantages of a higher resolution and better sinterability associated with a reduced porosity of the produced parts. The stabilization of the powder bed through a gas flow has been shown to be a promising method to compact the powder bed, increase the green part density and to enable the spreading of very fine powders [9]. The effects of the stabilization of the powder bed through a gas flow have been evaluated by 3D printing tablets and scaffolds made of α-TCP. Fine (< 25 μm) and coarse (45–100 μm) powder of α-TCP have been synthesized from $CaCO_3$ and H_3PO_4 and they have been compared to study the printing capability with and without the application of the gas flow. Tablets and scaffolds have been printed and investigated regarding achieved densities and mechanical properties.

2. Material and methods

2.1. Material synthesis

α-TCP was obtained by solid state reaction starting from $CaCO_3$ (calcium carbonate, d = 14 μm, EMSURE®, Merck) and H_3PO_4 as 85% aqueous solution (ortho-phosphoric acid 85%, assay (alkalimetric) ≥ 85.0%, EMSURE®, Merck). Seven batches were prepared, each with a theoretical mixture of 193.62 g $CaCO_3$ and 88.02 ml H_3PO_4 (85%). After pouring and mixing H_3PO_4 (85%) in $CaCO_3$, the mix was dried overnight in an oven at 100°C. Then, once the powder was milled with a mortar to achieve a fine, uniform powder, it was heat treated in a Pt–Ir crucible. The powder was heated with a rate of about 600°C/h, with dwelling times at 400°C, 800°C and 1000°C of 1 h each. Air quenching followed the last dwelling step. Afterwards, the powder was milled again with a mortar and heated up 1600 °C for 2 h in a Pt–Rh crucible. At the end the powder was air quenched once more. Finally, the batches were combined and the obtained compound was milled with a mortar and in a ball mill. The powder was subsequently sieved into two fractions: lower than 25 μm, which is typically critical to process and between 45 and 100 μm, which is typically suitable to process. For simplicity, the paper will refer to these two sizes as fine and coarse powder respectively in the following. The synthesized powder was characterized by X-ray diffraction (XRD) using CuKα radiation at 40 kV and 40 mA over an angular range of 5–80° with a step size of 0.02° 2Θ (D8 Advance with Bragg-Brentano geometry, Bruker AXS GmbH, Germany). In addition, the particle size distribution was determined using a particle size analyzer (Mastersizer S, Malvern Instruments GmbH, Herrenberg, Germany) and the shape of powder particles was investigated by scanning electron microscopy (SEM, ZEISS

Gemini Supra 40, Carl Zeiss AG, Oberkochen, Germany).

2.2. Printing

To print the powder, a commercial 3D printer was used (RX-1, ExOne, USA). It comprises two powder boxes as illustrated in Fig. 1. One is the feed bed where the feedstock powder is accomodated and applied via a roller to the build bed, which is illustrated on the right and it moves down by the thickness of one layer. Each bed measures 7 × 5 × 2.5 cm. This commercial setup was modified by connecting a rotary vane pump for low vacuum (Pfeiffer vacuum, Duo 10M) to the build platform. The resulting gas flow throughout the powder bed leads to a higher compaction of the powder, since the associated draft acts in the same direction of the gravitational force. The building platform is made of a porous sinter-steel filter with a mean porosity of 10 μm to enable the air suction through the powder bed. Further information on the setup are available in Patent US9533452B2 [10].

The geometries chosen for printing are tablets and scaffolds as shown in Figs. 2 and 3. The tablet measures 15 mm in diameter and 3 mm in height, while the cubic shaped scaffold has a designed porosity with squared cells of 2 mm sides and struts of 1 mm.

As binding liquid, the commercial binder PM-S-SR2-05 by ExOne is used. It is delivered from the storage tank to the printhead through a peristaltic pump and jetted by a Fujifilm SE 128 AA printedhead with 128 selectively activated nozzles to the powder bed.

Printing was followed by a sintering program. The parts were dwelled for 2 h at 450°C to burnout the binder and subsequently for 6 h at 1600°C for sintering. The heating and cooling rate was 10°C/min. Phase transformation behaviour was investigated by differential thermal analysis (DTA, STA 409, Netzsch, Selb, Germany).

2.3. Characterization

The powder bed density was determined to estimate the density of the green part (printed and unsintered). Therefore, a certain number of powder layers (50 layers, each layer 105 μm thick) were deposited on the build plate. Afterwards, the volume of the build area covered with powder was calculated and the powder was collected to measure its mass. By dividing the mass of the spread powder by the volume it occupies in the build bed the powder bed density is determined. The density and porosity of the printed and sintered tablets were determined according to the Archimedes' method (ISO 18754) removing the air from the pores through vacuum. The solid density was also confirmed by helium pycnometry (Pycnomatic ATC, Nuova A.E.Z. Srl, Camburzano, Italy). By X-ray computer tomography (μCT 40, Scanco Medical AG, Switzerland), porosity as well as geometrical defects of the printed tablets were visualized. Optical microscopy (OM) was performed on parts embedded in epoxy resin and polished afterwards, to evaluate and compare the microstructure. The mechanical properties were evaluated with the ball on three balls test (B3B) for the tablets, and by a compression test for the cubes (Z005, Zwick/Roell, Ulm, Germany). The radius of the balls used was 5.5 mm, the test started after a preload of 3 N and the rate was 0.01 mm/min. The Poisson ratio used for α-TCP was 0.25. For the compressive test, the preload was 1 N and the rate 0.5 mm/min. As comparison to the printed tablets, pressed tablets were also produced both with coarse and fine powder (16 mm in diameter and 3 mm in height), using a preload of 5 kN and final pressing with 10 kN for 30 s. After sintering they underwent B3B testing as well.

3. Results and discussion

3.1. Material synthesis

The XRD analysis confirmed that the phase assemblage of the produced powder comprised mainly α-TCP. In Fig. 4, the XRD patterns of the seven batches, termed α-TCP 1 to α-TCP 7, as well as the α-TCP (red) and
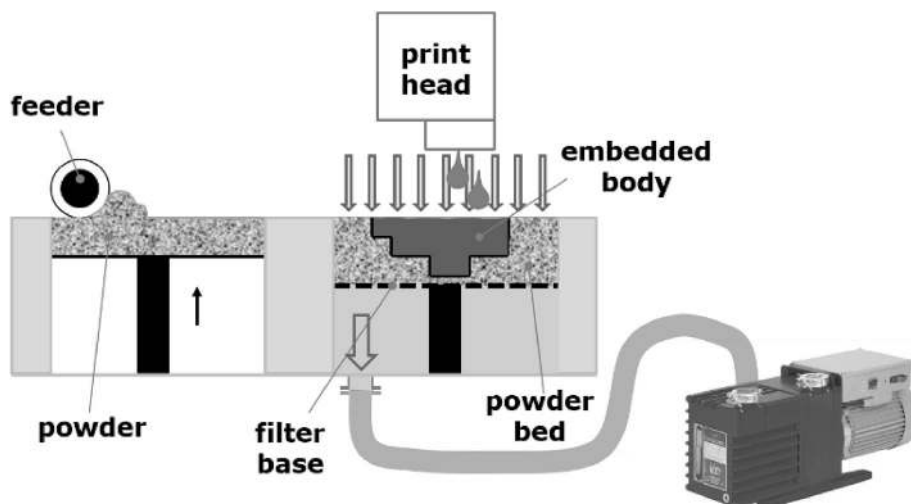
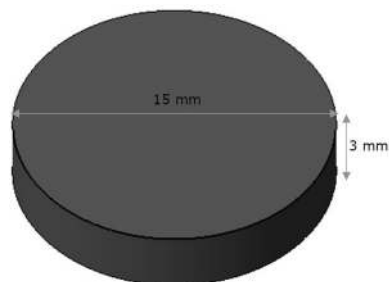**Fig. 1.** Set up of gas flow assisted powder deposition.

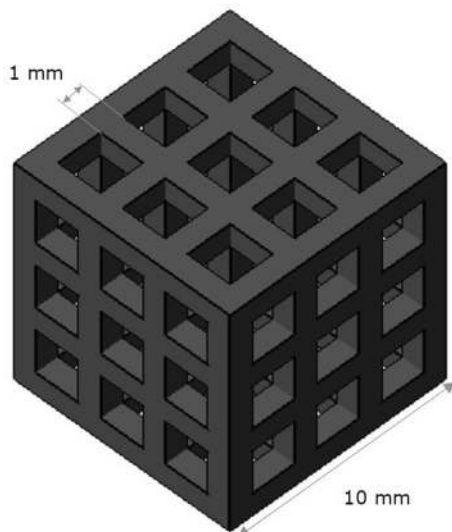**Fig. 2.** 3D model and dimensions of the tablet.

Fig. 3. 3D model and dimensions of the scaffold.

HA (blue) standard pattern are shown. The quantitative evaluation by the Rietveld method revealed amounts of Hydroxyapatite in a range from 0.5 to 3.5% in the single batches, leading to an amount of $98 \pm 2\%$ α-TCP and $2 \pm 1\%$ HA in the final compound. The presence of HA (relevant peaks highlighted) may occur due to an excessive amount of H_3PO_4 mixed with $CaCO_3$. Therefore, the ratio Ca/P is slightly higher than 1.5, which would be the required ratio to achieve pure TCP. This was also confirmed by ICP-OES analysis: the ratio Ca/P measured was 1.54. Any trace elements

as listed in ASTM F1088-04a were not detected.

Particle size investigation of the two powder fractions showed a particle size distribution of $d_{50} = 9$ μm and $d_{90} = 24$ μm for the fine powder sieved to lower than 25 μm and a particle size distribution of $d_{50} = 49$ μm and $d_{90} = 103$ μm for the coarse powder between 45 and 100 μm. The shape of the particles was investigated with SEM, and is presented in Fig. 5, showing the irregular form as a result of the grinding process with a ball mill.

3.2. Printing

Layer deposition tests were carried out to select the proper printing parameters for the setup with and without gas flow by varying the recoating speed, layer thickness (LT) and feed to layer thickness ratio (FLT). The feed to layer thickness ratio describes the amount of powder which is applied from the feed bed to the build bed. This is typically more than needed for one layer, to assure a fully covered and homogeneous powder layer in the build bed. The ratio usually varies between 1.5 and 3.

With the coarse powder, both with and without gas flow, the bed was homogeneously spread with a wider range of parameters. With the gas flow a slight texture on the surface was visible due to the metal filter that may cause preferential air channels in the powder bed. The parameters chosen for the coarse powder were LT = 105 μm, FLT = 2 and bed speed 10 mm/s for printing without gas flow and LT = 105 μm, FLT = 2.5 and bed speed 50 mm/s for printing with gas flow. More interestingly, the spread tests of the fine powder emphasized the effect of the gas flow. The fine powder cannot be deposited without gas flow since the bed is not uniform. The powder tends to agglomerate in front of the roller due to the high inter-particle forces. Varying different printing parameters does not affect significantly the results. On the other hand, when the powder bed is stabilized with the gas flow, the fine powder can be well spread with a smoother surface finish compared to the coarse powder. The printing parameters selected were LT = 105 μm, FLT = 3 and bed speed 10 mm/s. Printing with the fine powder required the installation of a sponge brush on top of the roller to avoid the contamination of the just flattened powder bed by agglomerations, as the finer particles have a higher tendency to adhere and attach to the roller. To sum up, three typologies of powder settings were used: 1. coarse powder printed without gas flow, 2. coarse powder printed with gas flow and 3. fine powder printed with gas flow. Sintering and debinding was performed on the parts. With the chosen heating and cooling rate of 10 °C/min, only the transformation between α and α' was observed around 1460°C and no reverse transformation to β-TCP was observed from DTA analysis. Fig. 6 shows the analysis of the coarse powder with a heating and cooling rate of 10°C/

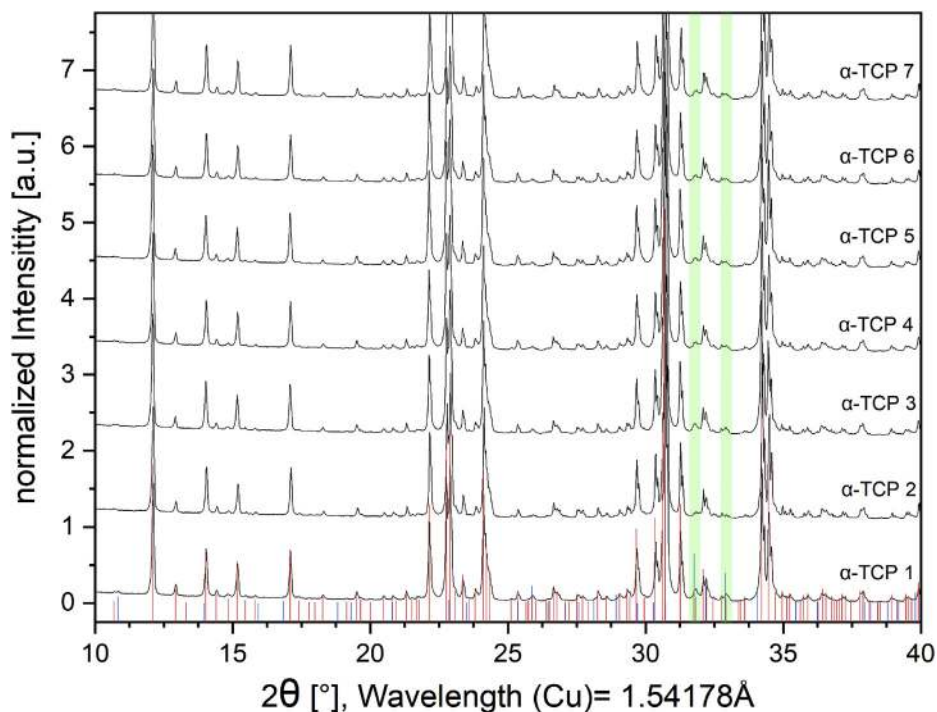**Fig. 4.** Normalized XRD patterns of the seven batches of the synthesized α-TCP powder with standard references of α-TCP (PDF 01-070-0364) in red and HA (PDF 01-076-0694) in blue.
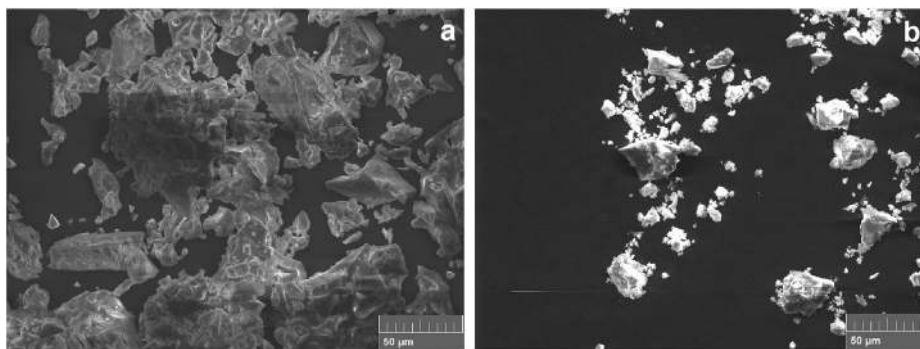

Fig. 5. SEM images of coarse (a) and fine (b) α-TCP powder.

min and a dwelling time of 20 min at 1570°C. The main transformation is from α- to α′-TCP at around 1464°C, visible from the endothermic peak during heating and the reverse transformation visible in the upward exothermic peak during cooling. The phase transformations occurred without significant mass change. DTA analysis of the fine powder revealed the same transformation behavior. In addition, a small peak is visible at around 200°C, both during heating and during cooling. This could be related to the HA (monoclinic, $P2_1/b$ according to XRD analysis) content in the material. A reversible transition of monoclinic HA to hexagonal symmetry ($P6_3/m$) is reported in literature. Ikoma et al. [11] observed it to take place at 207°C during heating and at 204°C during cooling.

3.3. Characterization

To evaluate the powder behaviour during printing, the different powders were characterized prior to printing, as shown in Table 1. Powder bulk density (freely settled and tapped), Hausner ratio and powder bed density were determined and listed with standard deviation. The Hausner ratio is calculated from the tapped density and the freely settled density of the powder [12]. A value close to one means that the flowability is excellent while a ratio around 1.50 represents a very poor flowability resulting in an irregular deposition. In brackets, the respective relative density in relation to the theoretical density is also listed. A higher flowability generally results in a higher packing rate.

The Hausner ratio of the coarse powder was lower and the packing rate higher than for the fine powder. The Hausner ratio of the fine powder (1.55) reflects the outcomes of the deposition tests: a poor flowability is acting against a good deposition. From Table 1 we can observe that the powder bed density was significantly affected by the stabilization of the gas flow. Focusing on the coarse powder, with gas flow the density increased from 36.0% to 43.9%. The fine powder with gas flow had a powder bed density in between that for the two types of coarse powder. With gas flow, the compaction of the fine powder was lower than that of the coarse powder, due to the high inter-particle attraction. Nonetheless, without gas flow the fine powder could not be deposited uniformly at all.

The density and porosity measurements of the printed and pressed tablets after sintering are shown in Figs. 7 and 8. All results are reported as mean ± standard error. Gas flow application during printing affected
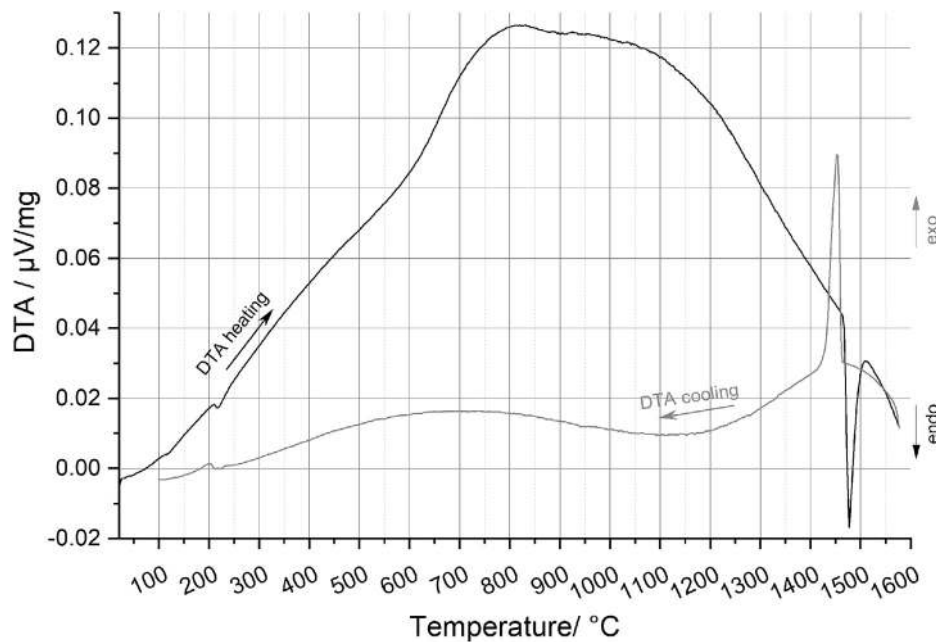
Fig. 6. DTA of the coarse powder with a cooling rate of 10°C/min.

Table 1
Powder properties.

Powder	Coarse	Fine
Bulk density		
freely settled [g/cm^3]	1.10 ± 0.03 (38.5 %)	0.71 ± 0.04 (24.9 %)
tapped [g/cm^3]	1.50 ± 0.04 (52.2 %)	1.10 ± 0.07 (38.6 %)
Hausner ratio	1.36 ± 0.04	1.55 ± 0.04
Powder-bed density		
without gas flow [g/cm^3]	1.03 ± 0.04 (36.0 %)	n.a.
with gas flow [g/cm^3]	1.26 ± 0.08 (43.9 %)	1.13 ± 0.01 (39.3 %)

the apparent solid density, bulk density and apparent porosity. Regarding the apparent density shown in Fig. 7 for the tablets made using the coarse powder (apparent solid volume considers solid volume and closed pore volume), the values were similar and they correspond to more than 99% of the density of the powder (2.857 g/cm^3 measured by pycnometer). This means that the amount of closed porosity was very low for these tablets, and the different preparation methods did not have a great influence on the formation of closed pores. The tablets obtained with fine particles had a lower apparent solid density than the ones made with

coarse powder. Moreover, the denser the tablets (those pressed), the lower the apparent density and therefore the higher the amount of the closed pores formed during sintering. Indeed, the denser the part, the harder to eliminate the closed pores, especially if the sintering process occurs without viscous flow. The results of helium pycnometry measurements to determine the density of the solid material are displayed in Fig. 7 for comparison. The results are in good agreement to the apparent solid density derived from Archimedes measurement.

Focusing on the bulk density presented in Fig. 7 (bulk volume considers solid volume, closed pore volume and open pore volume), the tablets with the fine particles had the highest values, corresponding to 91.7% (for the pressed tablets) and 81.9% (for the printed tablets) of the density of the fine powder (2.865 g/cm^3 measured with the pycnometer). For the tablets printed with coarse powder, the pressed tablets had the greatest density followed by the printed ones (with gas flow and then without gas flow). We can therefore note that gas flow reduced the overall porosity in the tablets.

The apparent porosity, shown in Fig. 8, is in agreement with the predictions: pressed tablets showed the lower amount of apparent porosity (higher effect with fine powder) and the tablets printed with fine particles and with gas flow had fewer open pores. Therefore, the
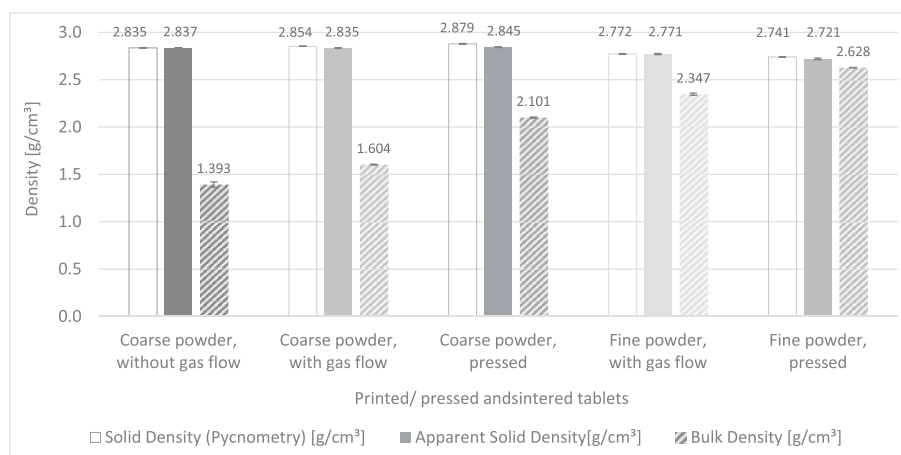

Fig. 7. Solid density (by Pycnometer), apparent solid density and bulk density (by Archimedes) of printed/pressed and sintered tablets.
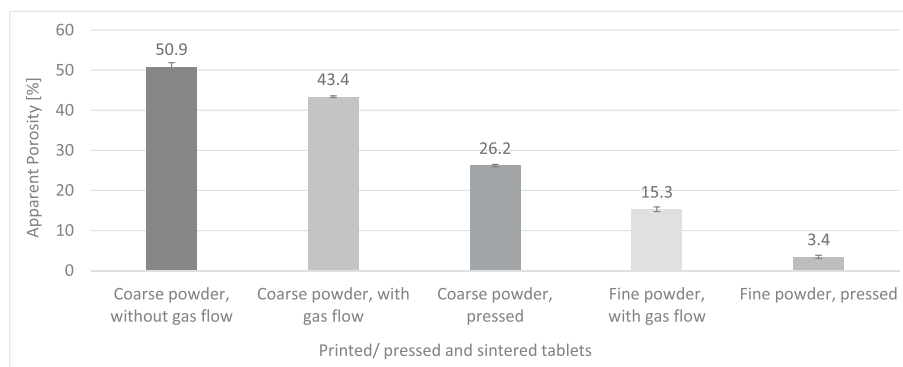
Fig. 8. Apparent porosity of printed/pressed and sintered tablets.

combination of the stabilization of the powder bed through a gas flow and fine particles allows to obtain denser printed parts, increasing the resolution during printing and the sintering activity. This is also visible from the μCT analysis performed on the printed and sintered tablets, as shown in Fig. 9. A more evident porosity can be observed throughout the entire volume in the tablets produced using coarse powder printed without gas flow (see Fig. 9a and b), whereas the amount of pores decreased from the center to the edge in the tablet printed using coarse powder with gas flow.

On the other hand, a higher densification during sintering is visible in the tablets printed with fine powder. The tablet shows the smallest amount of porosity, mainly localized in the center of the tablet. No gradients along the z-axis in the transversal sections could be seen in the tablets produced using coarse powder, indicating that the pressure of the gas flow was constant along the height (z printing direction). Instead, in the tablet produced using fine powder, the porosity seems to increase towards the upper surface. The radial gradient in density, which is slightly visible in Fig. 9b and becomes more prominent in Fig. 9d and f is related to the conventional sintering, where the thermal energy is transferred from the outside of the sample to the inside. Since all samples had the same sinter programm the effects of powder compaction due to the applied gas flow and the finer particles lead to higher densification rates in Fig. 9d and f. In addition, delamination of some layers can be observed in the tablet made of fine powder, especially close to the edges because of the higher stresses formed.

To check the strength of the tablets the ball on three balls test (B3B) was carried out, and the results are shown in Fig. 10 with standard error. Surprisingly, except from the tablet pressed with coarse powder, the strength was lower when the parts were denser. This can be explained by the presence of cracks in the samples. As revealed by the images obtained with optical microscope presented in Fig. 11, a higher amount of cracks is visible on the samples printed with fine powder and gas flow (Fig. 11 c,f). For the analysis, the tablets were embedded in epoxy resin (dark grey color) and polished.

The most likely reason for the formation of cracks is the transformation between α and α′ TCP phase at around 1460°C: this occurs with a change in density from 2.866 to 2.702 g/cm^3 during heating, accompanied by significant changes in the crystal structure. α-TCP is monoclinic (a = 1.2859 nm, b = 2.7354 nm, c = 1.5222 nm) and α' is hexagonal (a = b = 0.53507 nm, c = 0.7684 nm) [6] therefore this transformation may cause the formation of cracks due to the distortion of the lattice structure. The more porous parts can better relax the stresses formed and consequently fewer cracks are created and they have higher strength. The presence of cracks strongly affects the strength of the tablet since especially the tensile stress component promotes the elongation of the flaws. Generally, due to the low sintering activity of pure TCP, high temperatures are required. Since the finer particles have a better sinter behaviour, future investigations could focus on sintering at lower temperatures, to avoid such transformation. In addition, doping the material with elements like silicon for example can stabilize the α-TCP phase [13]

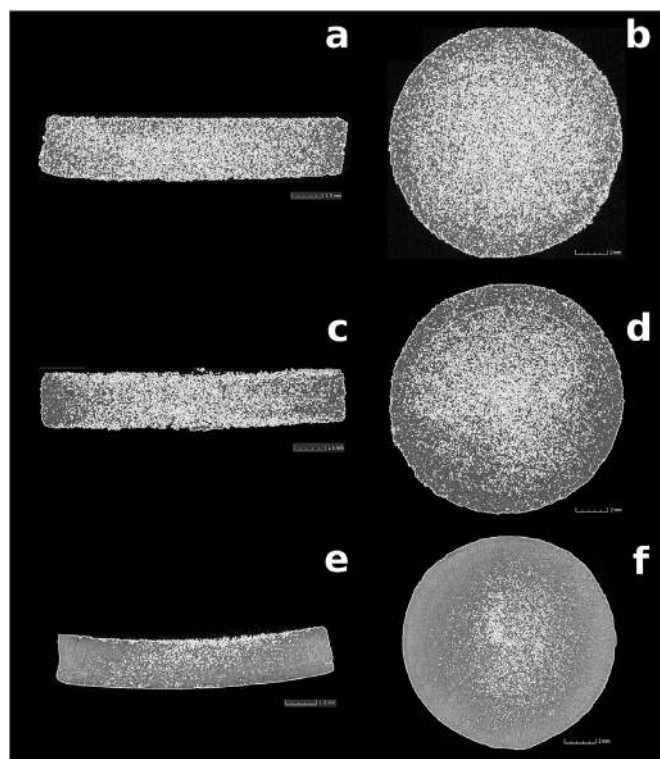**Fig. 9.** Transversal and longitudinal sections in μCT images of printed and sintered tablets (coarse powder without gas flow (a,b); coarse powder with gas flow (c,d); fine powder with gas flow (e,f).

and might be beneficial for the sinter process. Fig. 11 also allows conclusions to be drawn about the presence of open and closed porosity. Basically the open porosity corresponds to the resin used to embed the parts, which could penetrate in all pores due to the interconnectivity of the channels. On the other hand, the closed porosity coincides with the black spots since despite ultrasonic cleaning, abrasive solution used during the polishing remained in the pores. A high amount of closed pores is visible in the tablets printed with fine powder (Fig. 11c,f) compared to the one printed with coarse.

An investigation of the printed and sintered scaffolds with optical microscopy showed similar characteristics regarding the microstructure compared to the printed and sintered tablets. Printing with gas flow increases the density of the part, while the effect is higher with fine powder. Alike the tablets printed with fine powder, the fine scaffolds showed several cracks.

The bulk density of one printed and sintered scaffold per type was calculated from the ratio between the weight of the cube and the bulk
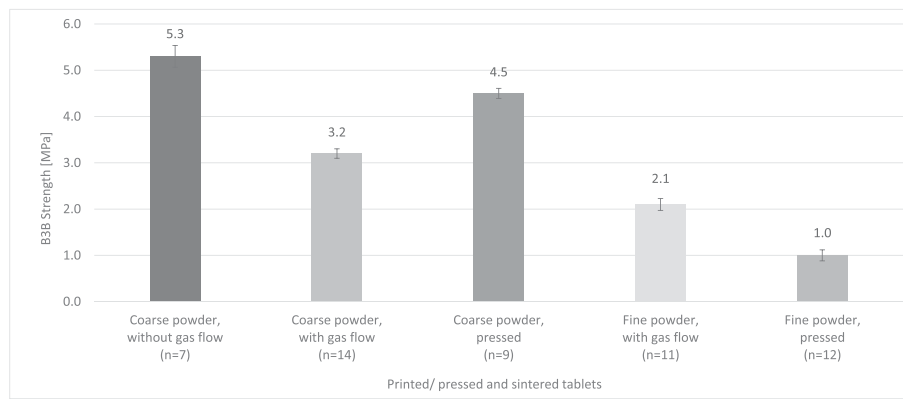
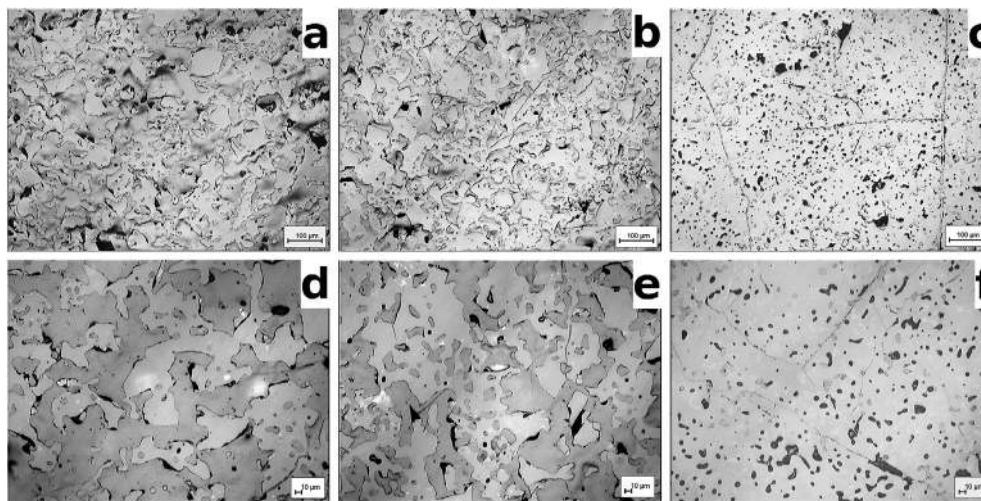**Fig. 10.** B3B strength of printed/pressed and sintered tablets with n representing the number of samples.

Fig. 11. OM images of printed and sintered α-TCP tablets - Coarse without (a,d), coarse with (b,e) and fine with (c,f) gas flow assisted powder deposition.

volume measured with the caliper. The results are depicted in Fig. 12. The cubes that were printed with fine powder and with gas flow assisted powder deposition show the highest bulk density, while the cube printed with coarse powder and no assistance of gas flow shows the lowest. The cubes were measured by helium pycnometry as well. The density of the solid material is in the range of the theoretical density for α-TCP. A slightly higher density can be noticed for the parts printed with coarse powder and gas flow compared to the printing without gas flow. Alike the tablets, the cube printed with fine powder and gas flow shows a slightly reduced density.
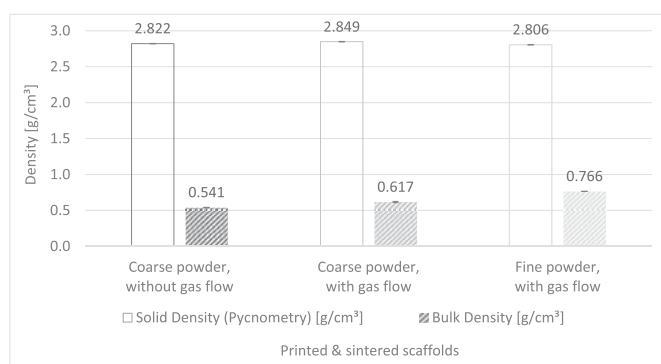

Fig. 12. Solid density and bulk density of the α-TCP printed and sintered scaffolds.

In addition, Fig. 13 shows the macroscopic designed porosity (the cells) of the three typologies of printed scaffolds. The vertical axis of the image matches the printing orientation (z axis) and the images show the printed surface after sintering. From these pictures, the better definition of the samples produced using fine powder can be observed (see Fig. 13c): the square of the cell is well defined and the amount of excessive powder along the sides is very low.

The mechanical properties of the sintered scaffolds were evaluated by compression. The results are shown in Fig. 14 with standard error. The scaffolds printed with fine powder with gas flow had the highest strength (3.4 MPa) followed by those printed with coarse powder with gas (1.5 MPa) and without gas (1 MPa). While for the B3B test the cracks are the defects causing the failure, in the compressive tests cracks tend to close and therefore the main parameter that controls the mechanical behavior is the density of the part. Consequently, the denser the part the greater the compressive strength. With a compressive strength of 3.4 MPa, the printed scaffolds produced in this work have a strength similar to that of cancellous bone, which ranges between 2-12 MPa. [14].

4. Conclusion

The aim of this study was to investigate the gas flow assisted Additive Manufacturing approach to achieve improved mechanical properties of bioceramic samples made of α-tricalcium phosphate. Therefore, tablets and scaffolds were printed using powders with a standard particle size between 45 - 100 μm and with a particle size below 25 μm, not suitable for standard (not assisted by gas flow) binder jetting printing. This study
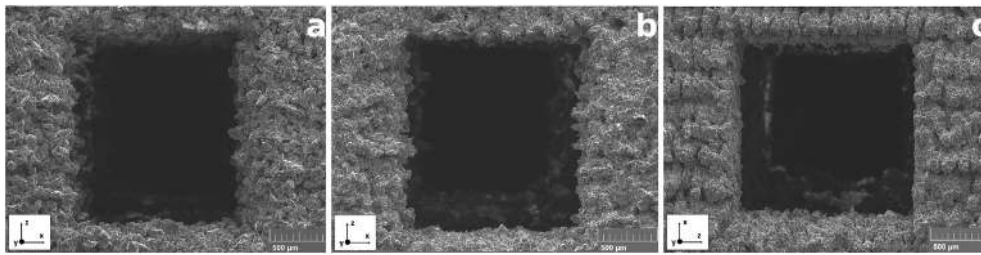
Fig. 13. SEM images of the cells of the α-TCP cubes: Coarse without (a), coarse with (b) and fine with (c) gas flow assisted powder deposition.
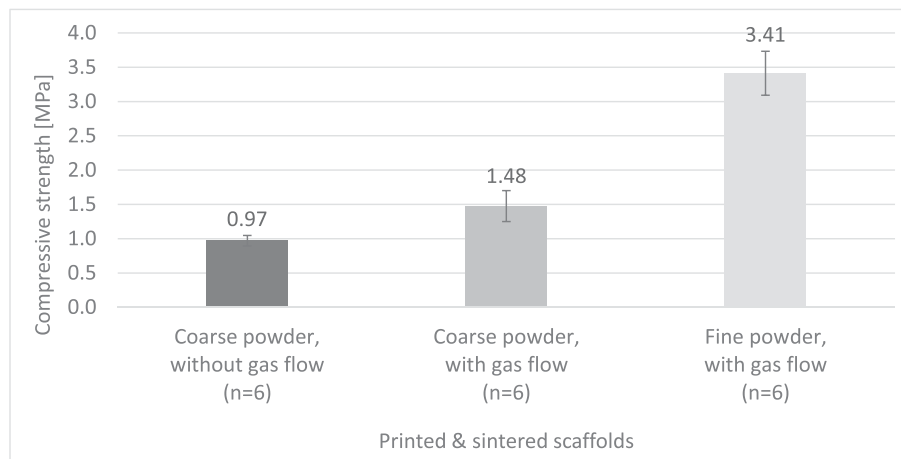

Fig. 14. Compressive strength of printed and sintered scaffolds with n representing the number of samples.

concluded that stabilization of the powder bed through a gas flow is essential for 3D printing of powder smaller than 25 μm, as it enables a uniform deposition and leads to a significant higher density of the printed part. It also improves the achievable resolution and positively influences the residual (after sintering) micro porosity of the printed parts. However, with the material chosen in this study, the higher density seems to promote a formation of cracks in the sample after sintering, that can strongly affect the mechanical properties. When looking at the behaviour of the printed test specimen under compression, the scaffolds printed with fine powder and gas flow assisted powder deposition possessed the best performance, despite the presence of cracks, attributable to the phase transformation of TCP from α to α'. Another advantage of using gas flow assisted powder deposition is that support structures, which are often used to avoid inclination of the printed part (especially of the first few layers) provoked by the friction generated by the movement of the recoater, are not required, thus reducing processing fabrication time and material waste.

Funding sources

Declaration of competing interest

The authors declare the following financial interests/personal relationships which may be considered as potential competing interests: The technology used in this publication is part of the patent US9533452B2. The co-author Jens Günster is one of the inventors.

References

[1] C.L. Ventola, Medical applications for 3D printing: current and projected uses, Pharm. Therap. 39 (10) (2014) 704–711.
[2] A.-V. Do, B. Khorsand, S.M. Geary, A.K. Salem, 3D printing of scaffolds for tissue regeneration applications, Adv. Healthc. Mater. 4 (2015) 1742–1762, https://doi.org/10.1002/adhm.201500168.
[3] M. Pilia, T. Guda, M. Appleford, Development of composite scaffolds for load-bearing segmental bone defects, BioMed Res. Int. doi:10.1155/2013/458253.
[4] L. Polo-Corrales, M. Latorre-Esteves, J.E. Ramirez-Vick, Scaffold design for bone regeneration, J. Nanosci. Nanotechnol. 14 (2014) 15–56, https://doi.org/10.1166/jnn.2014.9127.
[5] S.V. Dorozhkin, M. Epple, Die biologische und medizinische Bedeutung von Calciumphosphaten, Angew. Chem. (2002) 3260–3277.
[6] R.G. Carrodeguas, S.D. Aza, α-Tricalcium phosphate: synthesis, properties and biomedical applications, Acta Biomater. 7 (10) (2011) 3536–3546, https://doi.org/10.1016/j.actbio.2011.06.019, 10.
[7] S.V. Dorozhkin, Calcium orthophosphates (CaPO4): occurrence and properties, Prog. Biomater. 5 (2016), https://doi.org/10.1007/s40204-015-0045-z.
[8] S. Bose, S. Vahabzadeh, A. Bandyopadhyay, Bone tissue engineering using 3D printing, Mater. Today 16 (12) (2013) 497–504, 12.
[9] A. Zocca, C.M. Gomes, T. Mühler, J. Günster, Powder-bed stabilization for powder-based additive manufacturing, Adv. Mech. Eng. 6 (2014), https://doi.org/10.1155/2014/491581.
[10] J. Günster, A. Zocca, C. M. Gomes, T. Mühler, Method for Stabilizing a Powder Bed by Means of Vacuum for Additive Manufacturing. US patent No. 9533452B2, 2017.
[11] T. Ikoma, A. Yamazaki, S. Nakamura, M. Akao, Phase transition of monoclinic hydroxyapatite, Netsu Sokutei 25 (5) (1998) 141–149.
[12] H.H. Hausner, Powder characteristics and their effect on powder processing, Powder Technol. 30 (1) (1981) 3–8.
[13] M.J.S.A.M. Pietak, J.W. Reid, M. Sayer, Silicon substitution in the calcium phosphate bioceramics, Biomaterials 28 (28) (2007) 4023–4032, https://doi.org/10.1016/j.biomaterials.2007.05.003, 28.
[14] C. B. Carter, M. G. Norton, Ceramic Materials: Science and Engineering, Springer Science+Business Media New York, vol. 2. edn., ISBN 978-1-4614-3522-8, doi:10.1007/978-1-4614-3523-5.